A novel pre-processing technique for improving image quality in digital breast tomosynthesis

Hyeongseok Kim, Taewon Lee, Joonpyo Hong, and Sohail Sabir
Department of Nuclear and Quantum Engineering, Korea Advanced Institute of Science and Technology (KAIST), Daejeon 34141, Korea

Jung-Ryun Lee
School of Electrical and Electronics Engineering, Chung-Ang University, Seoul 06974, South Korea

Young Wook Choi
Korea Electricity Research Institute, Ansan 15588, South Korea

Hak Hee Kim and Eun Young Chae
Department of Radiology and Research Institute of Radiology, Asan Medical Center, University of Ulsan, College of Medicine, Seoul 05505, Korea

Seungryong Cho[a)]
Department of Nuclear and Quantum Engineering, Korea Advanced Institute of Science and Technology (KAIST), Daejeon 34141, Korea

(Received 9 August 2016; revised 20 December 2016; accepted for publication 20 December 2016; published 2 February 2017)

Purpose: Nonlinear pre-reconstruction processing of the projection data in computed tomography (CT) where accurate recovery of the CT numbers is important for diagnosis is usually discouraged, for such a processing would violate the physics of image formation in CT. However, one can devise a pre-processing step to enhance detectability of lesions in digital breast tomosynthesis (DBT) where accurate recovery of the CT numbers is fundamentally impossible due to the incompleteness of the scanned data. Since the detection of lesions such as micro-calcifications and mass in breasts is the purpose of using DBT, it is justified that a technique producing higher detectability of lesions is a virtue.

Methods: A histogram modification technique was developed in the projection data domain. Histogram of raw projection data was first divided into two parts: One for the breast projection data and the other for background. Background pixel values were set to a single value that represents the boundary between breast and background. After that, both histogram parts were shifted by an appropriate amount of offset and the histogram-modified projection data were log-transformed. Filtered-backprojection (FBP) algorithm was used for image reconstruction of DBT. To evaluate performance of the proposed method, we computed the detectability index for the reconstructed images from clinically acquired data.

Results: Typical breast border enhancement artifacts were greatly suppressed and the detectability of calcifications and masses was increased by use of the proposed method. Compared to a global threshold-based post-reconstruction processing technique, the proposed method produced images of higher contrast without invoking additional image artifacts.

Conclusions: In this work, we report a novel pre-processing technique that improves detectability of lesions in DBT and has potential advantages over the global threshold-based post-reconstruction processing technique. The proposed method not only increased the lesion detectability but also reduced typical image artifacts pronounced in conventional FBP-based DBT. © *2016 American Association of Physicists in Medicine* [https://doi.org/10.1002/mp.12078]

Key words: contrast enhancement, digital breast tomosynthesis, filtered-backprojection, histogram modification, image processing

1. INTRODUCTION

Breast cancer constitutes one of the most common causes of the mortality of women, and early detection of breast cancer is critically important for recovery.[1,2] Nowadays, digital breast tomosynthesis (DBT) plays a crucial role for breast cancer screening and diagnosis for its rich image information compared to mammography.[3–8] Mass and calcifications in the breast are major diagnostic targets in breast imaging. Particularly, a deposition of micro-calcification cluster (MCC) has a 70 to 85 percent chance to lead to cancer in the case of ductal carcinoma in situ.[9] In some cases, the calcifications are formed at the skin of breast and they are referred to dermal calcifications.[10,11] Typical artifacts of breast border enhancement in DBT images reconstructed by filtered-backprojection (FBP)

algorithm can cause missing or misclassifying such dermal calcifications.

DBT is a kind of computed tomography (CT) where a much less number of projections acquired from a limited scanning angle are used for image reconstruction. Because of this incompleteness of the scanned data, the DBT does not yield a quantitatively accurate 3D image information of the breast.[12–14] To enhance the image quality, various post-reconstruction processing techniques have been developed and widely used. It was reported that general image processing techniques which transform image globally often do not function properly because of various shapes and sizes of lesions in breast images. Therefore, regional or adaptive neighborhood methods have also been investigated with their successes to varying degrees upon situations.[15–19] CT is not in favor of a nonlinear pre-reconstruction processing such as histogram modification, because the projection data after such processing would violate the physics of image formation in CT thereby yielding inaccurate CT numbers. However, since the DBT fundamentally lacks the accuracy of the CT numbers and the detection of lesions is of highest concern in DBT, use of such a pre-processing can be justified as long as it improves DBT image quality more efficiently than those post-reconstruction processing techniques. In this work, we developed a novel pre-processing technique for DBT that results in a higher detectability and less image artifacts than a conventional image reconstruction.

2. METHODS

2.A. Histogram modification step

A pre-processing of histogram modification in this work was motivated to suppress the breast border artifacts in conventional DBT and to enhance the image contrast in the FBP algorithm framework. We developed our method in raw data domain to use the nonlinear property of a logarithmic function in our methodology. The reconstruction algorithm starts from converting the raw intensity data to the log-transformed data. Suppose I_0 and I represent the raw intensity of the background and the object, respectively. I_0 is typically acquired by taking projection without the object in the same scanning condition, and it has a spatial variation in the detector area in general. In this work, however, we use a fixed value of I_0 by taking the maximum value of the raw intensity of the background without loss of generality for the simplicity of the mathematical derivation of the proposed method. Then, $g=\ln(I_0/I)$ forms the log-transformed data that will be fed into the FBP engine. A ramp-type filtering in the FBP algorithm emphasizes high-frequency components of the data, and it leads to image artifacts such as brightened breast border when insufficient data from a limited-angle scan are used for image reconstruction as is the case for the DBT. Note that a relatively sharp breast boundary in the projection image constitutes a high-frequency component. Therefore, to mitigate the sharp transition of the breast border in the log-transformed data, we modified the histogram such that the background intensity gets closer to the object intensity. At the same time, the object histogram was also modified such that the intensity of the object shifts toward the lower values as an attempt to increase the contrast of the object's anatomical components in the log-transformed data. Figure 1(a) shows the histograms of the raw intensity data and Fig. 1(b) shows the line profile of g before and after histogram modification. Figure 1(c) is local line profile of g near boundary. As analyzed in the following, contrast in g'can be enhanced compared to g because of the property of logarithmic function.

The detailed procedures of the proposed method are now explained. First, we need to select the boundary value between background and breast bearing in mind that the breast border shall have a smooth transition to the background. As one can see in Fig. 1(a), there is a boundary region between breast and background. We selected a single value I_b, which will be representing the background, from the boundary region which has the lowest derivative of cumulative histogram as shown in Fig. 2.

After making the background to have the selected value I_b, we applied a uniform shift to the entire histogram by an amount of Δ. Let I_0' and I' represent the background and breast intensities after histogram modification. The log-transformed data before and after the histogram, g and g', would have the following relationship shown in Eq. (1) within the

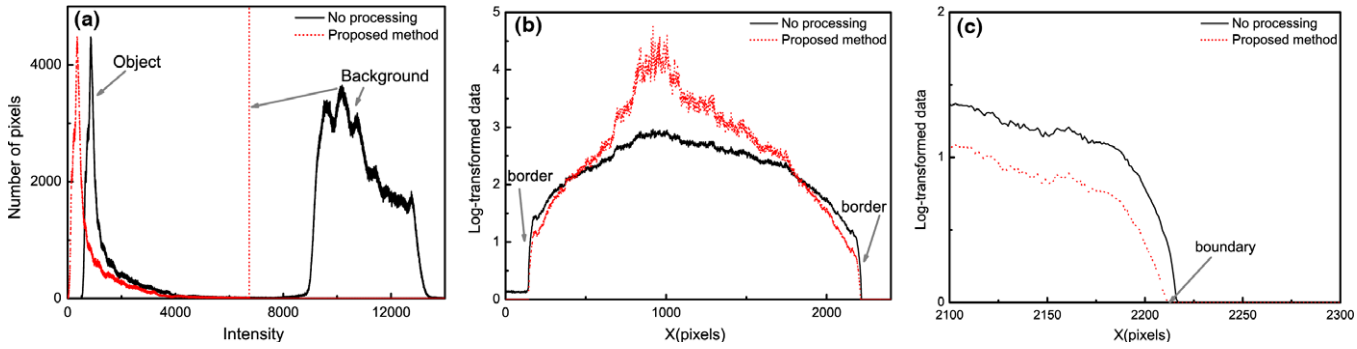

FIG. 1. (a) Histograms of the intensities in the first raw projection data, (b) example line profiles through the middle of the breast in the log-transformed projection data, and (c) the same line profiles in an enlarged scale near the breast border are shown in solid line (before the processing) and in dotted line (after the processing by the proposed method), respectively. [Color figure can be viewed at wileyonlinelibrary.com]

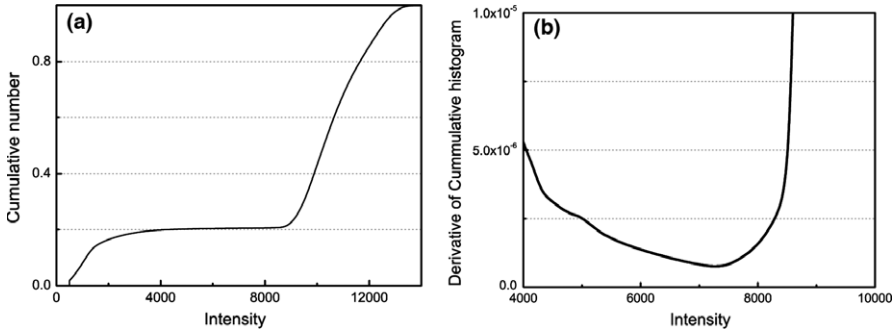

FIG. 2. (a) Cumulative histogram, (b) Derivative of cumulative histogram.

breast region. The second term in Eq. (1) has a constant negative value. The last term has a positive value depending on the value of I and the shift Δ. Since the denominator in the argument of the third term can be close to zero particularly when the attenuation of x-ray is relatively large, overall magnitude of the third term will be much larger than the second term. In addition, the second term will be constant throughout the image and will be effectively eliminated when one considers contrast as is shown in Eq. (2). This is how the contrast enhancement mechanism works in the proposed method. In addition, due to the histogram modification, the background projection value would be shifted near to the value of breast border projection. Without such a histogram modification, the log-transformed data would have a substantially large jump from the background to the breast border as summarized in Eq. (3) where ε represents an arbitrarily small value. Figure 1(c) visually demonstrates that the proposed method would produce a smoother transition near the breast boundary in the log-transformed data. This would help reduce the border enhancement related to the ramp filtering and the limited scan angle. We have selected Δ in this work such that the minimum intensity value becomes 1 after shifting the histogram. In other words, Δ was selected to be $I_{\min} - 1$.

$$\begin{aligned} g'(I) = \ln\left(\frac{I_0'}{I'}\right) &= \ln\left(\frac{I_b - \Delta}{I - \Delta}\right) = \ln\left(\frac{I_0}{I} \cdot \frac{I_b - \Delta}{I_0} \cdot \frac{I}{I - \Delta}\right) \\ &= \ln\left(\frac{I_0}{I}\right) + \ln\left(\frac{I_b - \Delta}{I_0}\right) + \ln\left(\frac{I}{I - \Delta}\right) \\ &= g(I) + \ln\left(\frac{I_b - \Delta}{I_0}\right) + ln\left(\frac{I}{I - \Delta}\right) \end{aligned} \tag{1}$$

$$\begin{aligned} g'(I_1) - g'(I_2) &= g(I_1) - g(I_2) + (\ln\left(\frac{I_1}{I_1 - \Delta}\right) \\ &\quad - \ln\left(\frac{I_2}{I_2 - \Delta}\right))(where\ I_1 < I_2) \\ &\geq g(I_1) - g(I_2) \\ &\left(\because \frac{I_1}{I_1 - \Delta} > \frac{I_2}{I_2 - \Delta} for\ any\ I_1, I_2\right) \end{aligned} \tag{2}$$

$$\begin{aligned} g'(I_b - \varepsilon) &= \ln\left(\frac{I_b - \Delta}{I_b - \varepsilon - \Delta}\right) \approx 0 \\ g(I_b - \varepsilon) &= \ln\left(\frac{I_0}{I_b - \varepsilon}\right) > g'(I_b - \varepsilon) \end{aligned} \tag{3}$$

2.B. Data acquisition

To demonstrate the performance of the proposed method, we have recruited clinical DBT projection data. A physical phantom (CIRS Model 010 & 011A) was also scanned by the DBT scanner following the same scanning condition as is used in clinical setting. The scanning parameters are summarized in Table I. Micro-calcifications and masses of the phantom and the patient's breasts have been used to evaluate the image quality. In addition, we synthetically inserted a calcification in the breast border region to see the effects of suppression of border enhancement in the proposed method.

2.C. Reconstruction algorithm

For image reconstruction, we used the conventional Feldkamp-Davis-Kress (FDK) that is tailored to the tomosynthetic image reconstruction. FDK algorithm is a cone-beam FBP algorithm expanded from a fan-beam algorithm. We have first converted our log-transformed data according to the virtual cone-beam geometry. Then, we performed data filtering in the Fourier domain by use of the modified ramp filter as will be detailed below, and back projection after filtering. Since the acquired data in a prototype DBT system occupy a double wedge-shaped space in the Fourier domain, we applied an asymmetric filter following the approach by Mertelmeier[20] for the ramp filter. The Fourier transform of the filter function H_{filter} can be written as

$$\begin{aligned} H_{filter}(\omega_y, \omega_z) = H_{sprectrum}(\omega_y) \cdot H_{profile}(\omega_z) \\ \cdot H_{inverse}(\omega_y, \omega_z), \end{aligned} \tag{4}$$

where $H_{inverse}$ is the inversion of modulation transfer function and is proportional to a ramp-like filter. The spectral filter $H_{spectrum}$ and the profile filter $H_{profile}$ can be written as

TABLE I. Scanning parameters.

Parameter	Value
kV	30
Current(mA)	45
Exposure Time	2500
mAs	112.5
Number of views	15
Pixel size	0.075 × 0.075 mm
Detector size	291 × 230 mm
Number of pixels	3888 × 3072

$$H_{spectrum}(\omega_y) = 0.5 \cdot (1 + \cos\frac{\pi\omega_y}{A}) \quad \text{for } |\omega_y| < A$$
$$= 0 \quad \text{elsewhere} \tag{5}$$

$$H_{profile}(\omega_z) = 0.5 \cdot \left(1 + \cos\frac{\pi\omega_z}{B}\right) \quad \text{for } |\omega_z| < B \text{ and } |\omega_z| < \tan\alpha\ |\omega_y|$$
$$= 0 \quad \text{elsewhere,} \tag{6}$$

where A and B regulate the cutoff frequencies in ω_y and ω_z.

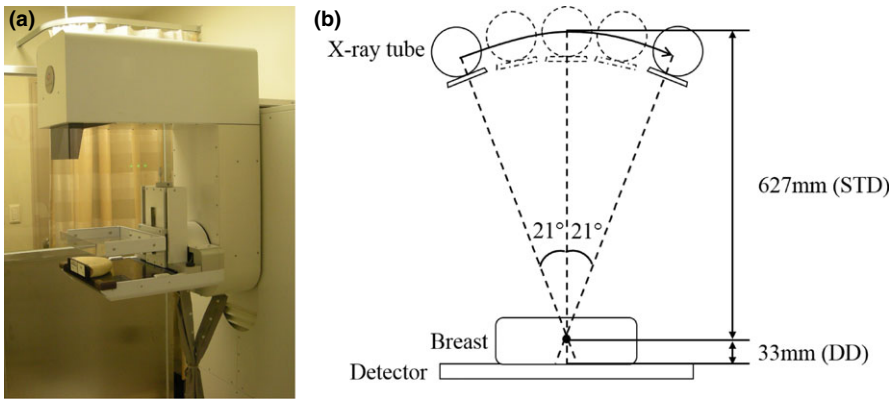

FIG. 3. (a) DBT system used in this work, (b) scanning geometry. [Color figure can be viewed at wileyonlinelibrary.com]

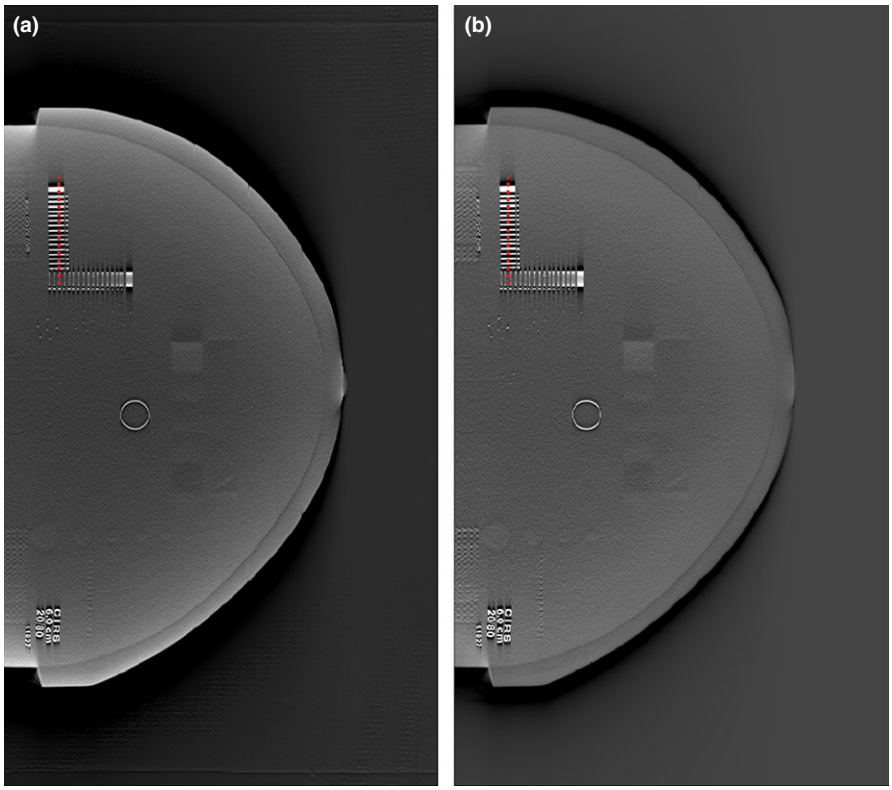

FIG. 4. Reconstructed image of quantitative phantom: (a) no processing, (b) proposed method. [Color figure can be viewed at wileyonlinelibrary.com]

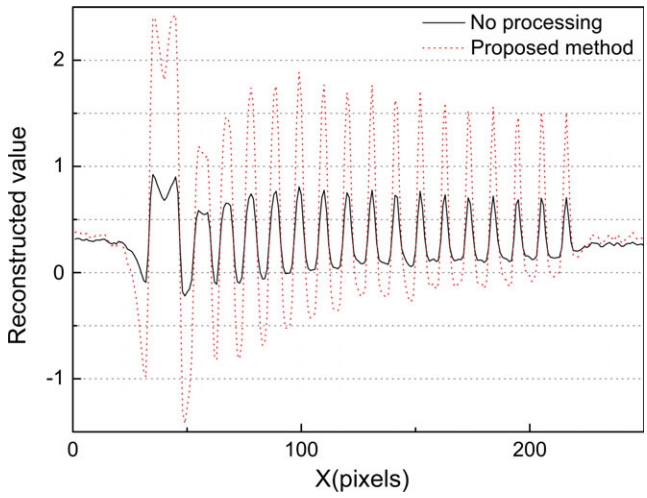

FIG. 5. Line profile of contrast bar in quantitative phantom. [Color figure can be viewed at wileyonlinelibrary.com]

2.D. Image quality assessment

For an image quality assessment, we computed the detectability index assuming an ideal model observer in the detection task.[21] The detectability d' is defined as

$$d'^2 = \sum_k \frac{|S(k)|^2}{P_c(k)}, \tag{7}$$

where $S(k)$ represents the discrete Fourier transform of the signal, and $P_c(k)$ represents the noise-power-spectrum (NPS) of the background. k denotes a discrete frequency vector in two-dimension. We calculated the NPS in the square-shaped ROIs at various positions on the image with their total number of L. Then $P_c(k)$ was calculated by

$$P_c(k) = \frac{1}{L}\sum_{l=1}^{L} |DFT\{W(g_l - g_{ave})\}|^2, \tag{8}$$

where DFT means the discrete fourier transform, W is a discrete window function to avoid over estimation of power at the edges of ROI,[22] and we used the Hanning window in this work. g_l and g_{ave} denote the image and the surface-fitted mean image within the l^{th} ROI, respectively. The right-hand side of Eq. (8) would be a function of spatial frequency k. In the CIRS phantom image, circular structures were directly calculated to yield its fourier spectral response. The relatively irregular structures in clinical images were rebinned by stacking normal line segments to the edges of the signal object. In other words, we collected several edge spread functions (ESFs) from the signal object boundaries, and aligned and averaged them to acquire a representative ESF. Using the averaged ESF, we have made a circularly symmetric blob to calculate the fourier spectral response of the signal. To calculate noise-power-spectrum, we used five background ROIs for each case. These ROIs were selected near the signals, and

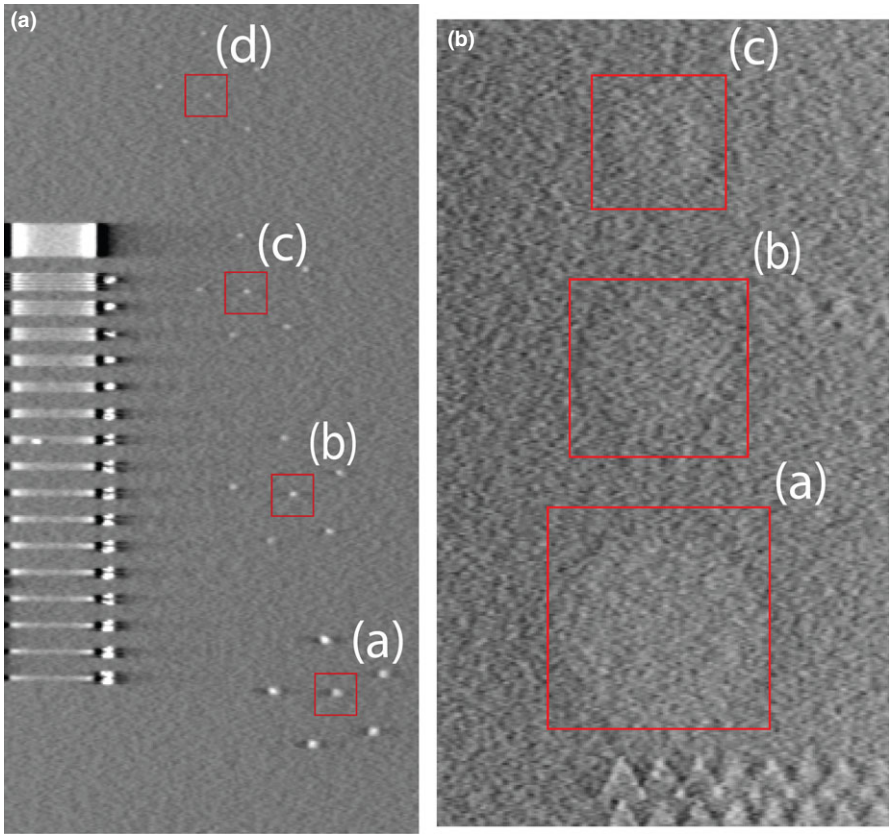

FIG. 6. Selected lesions in quantitative phantom: (a) micro-calcifications, (b) masses. [Color figure can be viewed at wileyonlinelibrary.com]

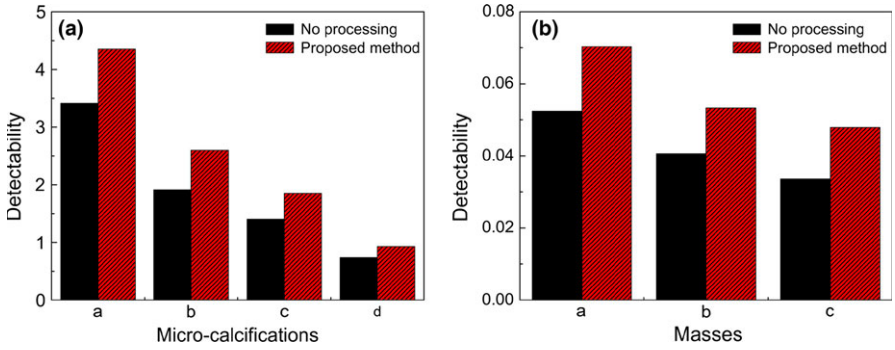

FIG. 7. Detectability of lesions in quantitative phantom: (a) micro-calcifications, (b) masses. [Color figure can be viewed at wileyonlinelibrary.com]

applied a surface-fit subtraction. Especially for clinical images, we selected the background near micro-calcifications, and we marked the ROIs used for the background NPS evaluation in Fig. 3.

3. RESULTS

Figure 4 shows the reconstructed images of the CIRS breast phantom from the data (a) without pre-processing and (b) with the proposed pre-processing. Display window is a critical component that determines a visual perception of a medical image, and it is desirable to use a consistent one when comparing two images. However, since the DBT images are inherently lacking quantitative accuracy in their output, particularly in our pre-processing type of work, it is difficult to use an objective unit such as CT number in the reconstructed image and a unified display window accordingly. We have therefore adjusted the display window in each comparative set of images to visualize the background tissue image similarly to our best capacity. A visual comparison would yield that the proposed method produces higher image contrast and much suppressed artifacts of border enhancement. In Fig. 5, we plotted the line profiles of the contrast bars across the dotted lines shown in Fig. 4.

For a more quantitative evaluation, we selected the structures simulating micro-calcifications and lesions as shown in Fig. 6 and calculated the detectability of them. The sizes of the micro-calcifications shown in Fig. 6 are (a) 400, (b) 275, (c) 230, and (d) 196 μm, respectively. The results are summarized in Fig. 7. It is clearly demonstrated that the proposed method increases detectability particularly for the high contrast objects with relatively bigger sizes.

We have also applied the proposed method to the clinical data. Figure 8 shows the reconstructed DBT slice images of a

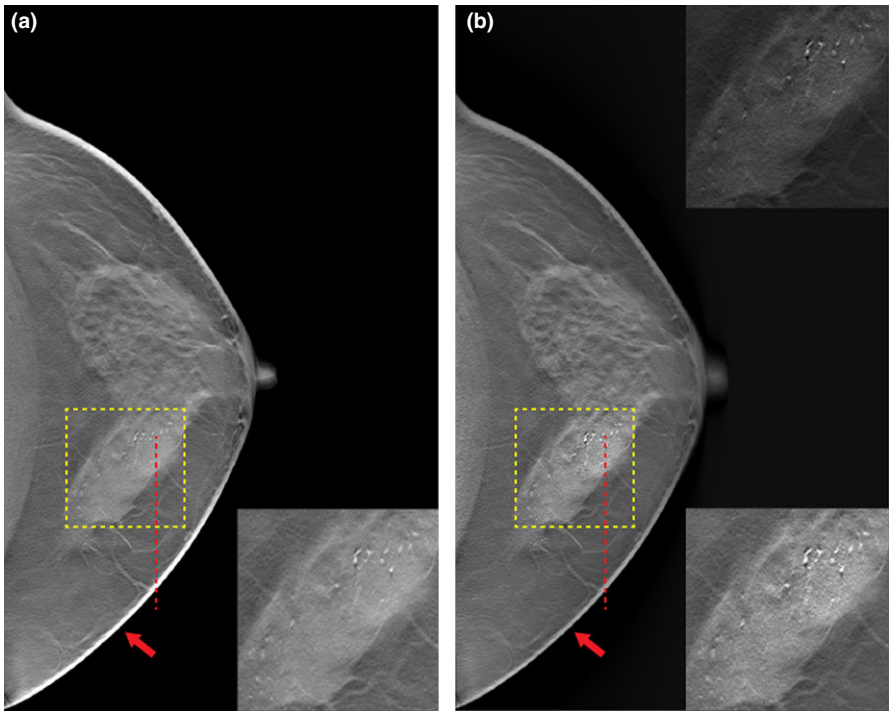

FIG. 8. Reconstructed DBT images: (a) no processing, (b) proposed method. The ROI image shown in the insert in the upper right corner of (b) is displayed with a different display window setting for comparison. [Color figure can be viewed at wileyonlinelibrary.com]

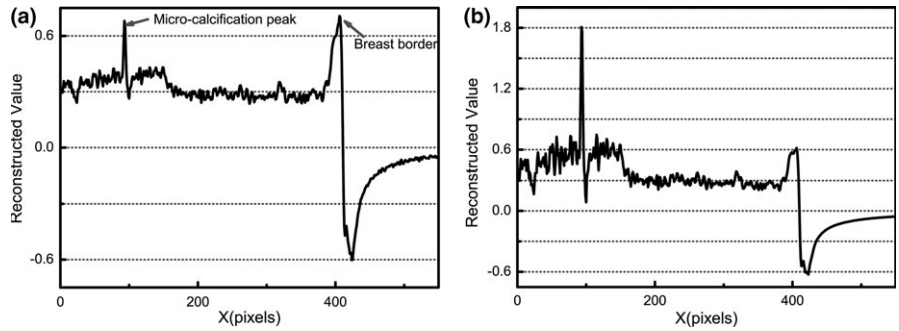

FIG. 9. Line profiles of DBT images: (a) no processing, (b) proposed method

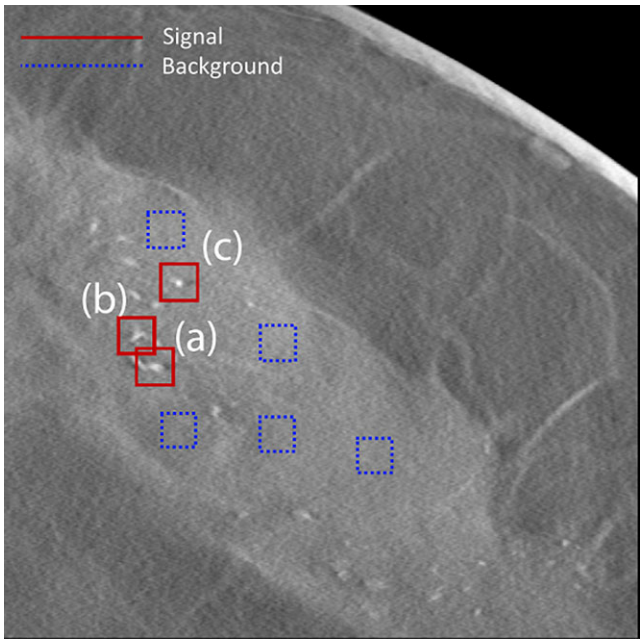

FIG. 10. Selected lesions in clinical data. [Color figure can be viewed at wileyonlinelibrary.com]

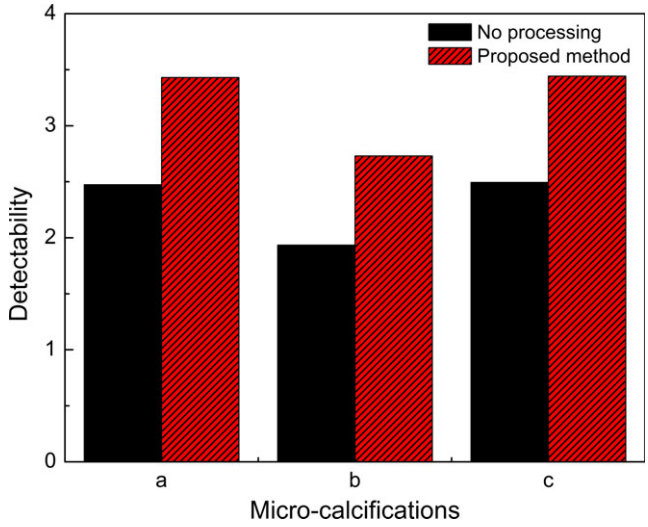

FIG. 11. Detectability of lesions in clinical data. [Color figure can be viewed at wileyonlinelibrary.com]

patient breast in craniocaudal (CC) view. As shown in Fig. 8, the visibility of micro-calcifications has been greatly improved in the image reconstructed by use of the proposed pre-processing method. In addition, the image artifacts of enhanced breast border have been substantially suppressed in the proposed method. In Fig. 9, we plotted line profiles along the dotted lines in Fig. 8 to better illustrate the contrast enhancement of micro-calcifications and the breast border suppression.

For a quantitative evaluation of clinical DBT images, we computed detectability of micro-calcifications which are marked with boxes in Fig. 10, and the results are summarized in Fig. 11. The sizes, in the full-width-half-maximum sense, of the micro-calcifications shown in Fig. 10 are estimated to be (a) 1500 (major axis) and 750 (minor axis), (b) 1000 (major axis) and 550 (minor axis), and (c) 650 μm, respectively. The detectability of micro-calcifications in the DBT images from the pre-processed clinical data also increased compared to the conventionally reconstructed images.

As an attempt to demonstrate the significance of breast border suppression, dermal calcification has been synthesized in the projection data as was explained in the methods part. In Fig. 12, the reconstruction results without and with the proposed pre-processing clearly show that the image contrast of the dermal calcification can greatly improve via the proposed method.

4. DISCUSSION

We were able to show that breast border artifacts can be greatly mitigated and that the image contrast of lesions can be improved by use of the proposed nonlinear pre-processing. Although it is true that the histogram modification would also contribute to increasing image noise as well as image contrast, due to the logarithmic nature of the data transformation in tomosynthesis the contrast enhancement would outweigh the noise increment after the histogram modification. The supporting evidences in terms of detectability evaluation have been found in both physical phantom images and clinical images. Since the signal enhancement outweighs the noise increase, the likelihood to increase the false positive rate is considered negligible. The visual perception strongly

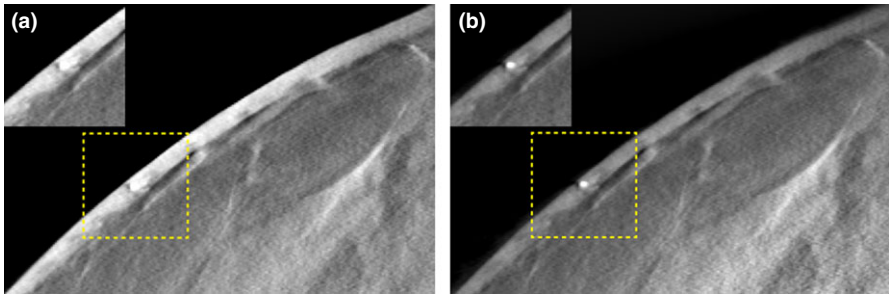

FIG. 12. Reconstructed images of dermal calcification simulation: (a) no processing, (b) proposed method. [Color figure can be viewed at wileyonlinelibrary.com]

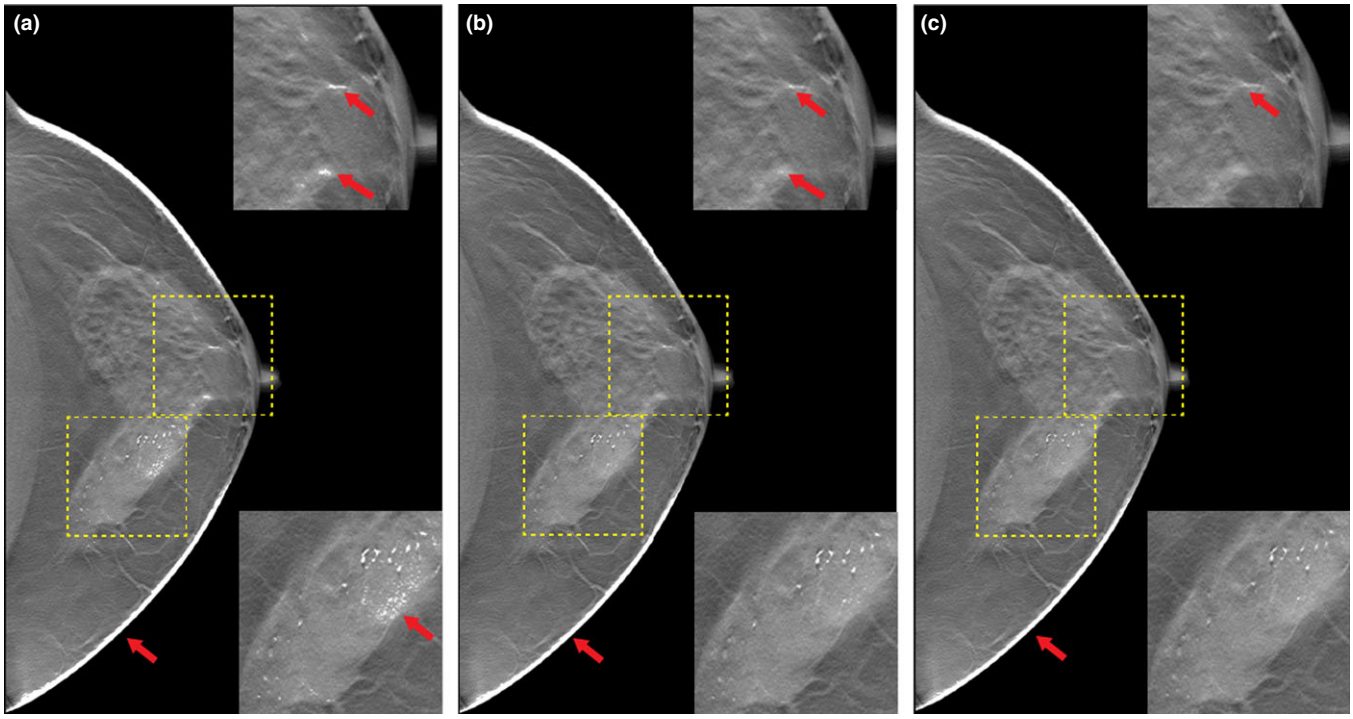

FIG. 13. Post-processed images with (a) low, (b) intermediate, and (c) high threshold values. [Color figure can be viewed at wileyonlinelibrary.com]

depends on the display window of an image, and it happens that the window setting we used in Fig. 8 appears to emphasize the image noise increment. The inserted ROI image in the upper right corner of Fig. 8(b) with a different display window setting implies that the proposed method would not overly enhance the noise leading to spurious structures being confused with real micro-calcifications. The proposed method attempts to suppress the breast border enhancement, and the nipples may appear to be distorted as a result. The nipple image indeed is enhanced in the conventional reconstruction approach as the nipple occupies a boundary region of the breast. However, we would like to note that the image information is still preserved without critical distortions and that the nipple image can be visualized in its optimum display window setting.

One may argue that an imaging performance enhancement of DBT can be achieved through post-reconstruction processing techniques. While we do not disagree that an optimized post-processing may lead to a similar or even better imaging performance compared to the proposed pre-processing method, we would like to emphasize that such an optimization often requires laborious task-specific tailoring procedures and more importantly that such post-processing techniques can be applied in parallel with the proposed pre-processing method synergistically.

To show limitations of a conventional post-processing technique, we implemented and applied a global threshold-based post-reconstruction processing to the reconstructed DBT images without pre-processing. Figure 13 shows the results of the implemented post-reconstruction processing with varying threshold values. As can be seen, contrast enhancement is achieved at smaller threshold values with substantial image artifacts. More structures are likely to be included in calcifications as false positives. With larger threshold values, this kind of image artifacts would be reduced while the image contrast of true lesions would not

gain either. In addition, the breast border artifacts would become even stronger after such a post-reconstruction processing since the breast border has a higher pixel values than the targets. As mentioned earlier, more sophisticated post-reconstruction processing techniques such as regional post-processing methods can possibly go around the problems of a global threshold-based post-processing. A full exploitation of such advanced post-processing techniques and an introduction of hybrid methods combining the pre- and post-processing techniques are, however, left for the future work.

We would like to add that the proposed method would be useful for the computer-aided-diagnosis (CAD) as well. CAD recruits a number of image features to classify suspicious lesions thereby providing a secondary opinion to the radiologists. Mean pixel values or shape descriptors of lesions are good examples of such image features. Enhanced breast border or reduced contrast of lesions in DBT images therefore can lead to a suboptimal performance of the CAD program. In addition, there are increasing interests in composing a mammogram from the DBT slice images in a hope that a DBT scan can provide mammographic image information as well to the radiologist negating the need of additional mammographic scans. We believe that the proposed pre-processing technique can help increase the clinical utility of such synthetic mammograms.

5. CONCLUSION

We have introduced a novel pre-processing technique that uses histogram modification to improve image quality of DBT and successfully demonstrated that the image detectability can be increased and that the breast border artifacts can be greatly suppressed.

ACKNOWLEDGMENTS

This study was supported in part by the MSIP grant NIPA-2014-H0301-14-1015, by the NRF grant 2013M3C1A3064457 and 2013M2A2A9043476, and by the NST grant CAP-13-3-KERI.

CONFLICT OF INTERESTS

The authors have no relevant conflicts of interest to disclose.

[a]Author to whom correspondence should be addressed. Electronic mail: scho@kaist.ac.kr.

REFERENCES

1. Jemal A, Siegel R, Xu J, Ward E. Cancer statistics, 2010. *CA Cancer J Clin*. 2010;60:277–300.
2. Champaign JL, Cederbom GJ. Advances in breast cancer detection with screening mammography. *Ochsner J*. 2000;2:33–35.
3. Gennaro G, Toledano A, Di Maggio C, et al. Digital breast tomosynthesis versus digital mammography: a clinical performance study. *Eur Radiol*. 2010;20:1545–1553.
4. Poplack SP, Tosteson TD, Kogel CA, Nagy HM. Digital breast tomosynthesis: initial experience in 98 women with abnormal digital screening mammography. *Am J Roentgenol*. 2007;189:616–623.
5. Andersson I, Ikeda DM, Zackrisson S, et al. Breast tomosynthesis and digital mammography: a comparison of breast cancer visibility and BIRADS classification in a population of cancers with subtle mammographic findings. *Eur Radiol*. 2008;18:2817–2825.
6. Zuley ML, Bandos AI, Ganott MA, et al. Digital breast tomosynthesis versus supplemental diagnostic mammographic views for evaluation of noncalcified breast lesions. *Radiology*. 2013;266:89–95.
7. Suryanarayanan S, Karellas A, Vedantham S, et al. Comparison of tomosynthesis methods used with digital mammography. *Acad Radiol*. 2000;7:1085–1097.
8. Haas BM, Kalra V, Geisel J, Raghu M, Durand M, Philpotts LE. Comparison of tomosynthesis plus digital mammography and digital mammography alone for breast cancer screening. *Radiology*. 2013;269:694–700.
9. Kang SH, Chung KY, Kim YS, Choi JS, Lee SS. Pathologic analysis of clustered microcalcification found on mammograms: a review of 77 cases. *J Korean Surg Soc*. 2004;66:5–9.
10. Pisano ED, Yaffe MJ, Kuzmiak CM. *Digital mammography*. ed. Philadelphia: Lippincott Williams & Wilkins; 2004.
11. Giess CS, Raza S, Birdwell RL. Distinguishing breast skin lesions from superficial breast parenchymal lesions: diagnostic criteria, imaging characteristics, and pitfalls. *Radiographics*. 2011;31:1959–1972.
12. Sechopoulos I. A review of breast tomosynthesis. part I. the image acquisition process. *Med Phys*. 2013;40:014301.
13. Niklason LT, Christian BT, Niklason LE, et al. Digital tomosynthesis in breast imaging. *Radiology*. 1997;205:399–406.
14. Baker JA, Lo JY. Breast tomosynthesis: state-of-the-art and review of the literature. *Acad Radiol*. 2011;18:1298–1310.
15. Morrow WM, Paranjape RB, Rangayyan RM, Desautels JEL. Region-based contrast enhancement of mammograms. *IEEE Trans Med Imaging*. 1992;11:392–406.
16. Rangayyan RM, Shen L, Shen Y, et al. Improvement of sensitivity of breast cancer diagnosis with adaptive neighborhood contrast enhancement of mammograms. *IEEE Trans Inf Technol Biomed*. 1997;1:161–170.
17. Kim JK, Park JM, Song KS, Park HW. Adaptive mammographic image enhancement using first derivative and local statistics. *IEEE Trans Med Imaging*. 1997;16:495–502.
18. Gordon R, Rangayyan RM. Feature enhancement of film mammograms using fixed and adaptive neighborhoods. *Appl Opt*. 1984;23:560–564.
19. Dhawan AP, Gianluca B, Richard G. Enhancement of mammographic features by optimal adaptive neighborhood image processing. *IEEE Trans Med Imaging*. 1986;5:8–15.
20. Mertelmeier T, Orman J, Haerer W, Dudam MK. Optimizing filtered backprojection reconstruction for a breast tomosynthesis prototype device. *Proc SPIE*. 2006;6142:61420F–61420F-12.
21. Barrett HH, Yao J, Rolland JP, Myers KJ. Model observers for assessment of image quality. *Proc Natl Acad Sci USA*. 1993;90:9758–9765.
22. Bian J, Siewerdsen JH, Han X, et al. Evaluation of sparse-view reconstruction from flat-panel-detector cone-beam CT. *Phys Med Biol*. 2010;55:6575–6599.